Shear stress dependency of small strain stiffness and creep of Toyoura sand

La dépendance de la cisaille contrainte, de la petite déformation raideur et le fluage du sable de Toyoura

J.Kuwano & S.K.Chaudhary – *Department of Civil Engineering, Tokyo Institute of Technology, Japan*
S.Hashimoto – *Kumagai Gumi Co., Ltd. (formerly Tokyo Institute of Technology), Tokyo, Japan*

ABSTRACT: Hollow cylinder torsion shear tests have been carried out to study anisotropy of small strain stiffness and creep of dense Toyoura sand under various shear stress conditions in the p'-constant plane. Amounts of creep strain and creep strain rate are correlated with the shear stress level as well as the shear direction. Small strain stiffness components are measured by applying small amplitude cyclic loads. The power low of stress is adapted to the test data to express the shear stress dependency of small strain stiffness. Contour lines of modulus are drawn in the p'-constant plane to see overall shear stress dependency of the stiffness.

RÉSUMÉ: Des tests de cisaillèment en torsion de cylindres creux ont été menes pour étudier l'anisotropie de petites contraintes de dureté et de fluage sur du sable dense de Toyoura, sous différentes conditions de pression avec cisaillèment dans le plan ap' constant. Les contributions du fluage ainsi que le taux de fluage ont été corréles avec le niveau des contraintes de cisaillèment, comme avec leur direction. Les petites composantes des contraintes de dureté ont été mesurees en appliquant des charges cycliques de faible amplitude. La loi de puissance de la pression est ajustée aux données des tests pour caractériser la dépendance des petites contraintes de dureté avec le cisaillèment. Le lignes de contour du module sont tracées dans le plan a p' constant pour faire apparaître la dépendance de la dureté en fonction des contraintes de cisaillèment.

1 INTRODUCTION

It is essential to properly estimate the deformation characteristics of soils for a successful prediction of ground movements. Soil is known to show non-linear and inelastic deformation properties. On the other hand, it has been recognized recently that the ground strains in field cases are generally less than about 0.5% and the small-strain stiffness of soil is important in the ground deformation analysis (Burland 1989, Atkinson 2000). Non-linearity and elasticity have been studied extensively and incorporated into various models. Another characteristic feature of soil is anisotropy of strength and stiffness because of non-spherical particle shapes, directionally distributed contact planes between particles developed at the time of deposition in the gravitational field, and so on (e.g. Oda 1972). However, anisotropy of soil in the wide range of strain is not fully investigated. In recent years, anisotropy at small strains in so called elastic region has been studied by some researchers using body wave measurements (Bellotti et al. 1996, Kuwano et al. 1997, Jovicic & Coop 1998) and locally instrumented triaxial tests (Hoque & Tatsuoka 1998). But only few studies have been carried out over the non-linear range and under general stress conditions (Zdravkovic & Jardine 1997, Nakamura et al. 1999). Viscous behavior of soil is also a characteristic feature of soil. Although creep behavior of sand has not been recognized in the normal practice, it may not be neglected in a small strain range (Shibuya et al. 1991, Di Benedetto & Tatsuoka 1997). In this study, Shear stress dependency of small strain stiffness and creep of Toyoura sand were investigated by using the hollow cylinder apparatus.

2 TEST OUTLINE

A hollow cylinder apparatus with the specimen dimensions of h = 20cm, r_i = 3cm, r_o = 5cm was used in this study. Four stress components, σ_z, σ_θ, σ_r and $\tau_{z\theta}$, can be controlled independently by applying axial load, W, torque, M_T, inner cell pressure, p_i, and outer cell pressure, p_o, to the hollow cylinder specimen as shown in Figure 1. Four strain components, ε_z, ε_θ, ε_r and $\gamma_{z\theta}$ can be measured in this apparatus. Vertical strain, ε_z, and shear strain in

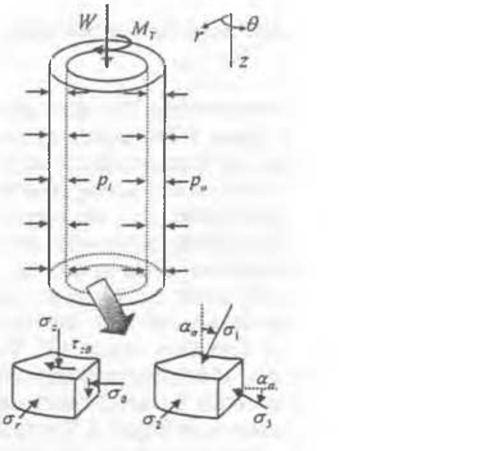

Figure 1. Stress components in hollow cylinder apparatus.

z-θ plane, $\gamma_{z\theta}$, are measured by proximity transducers at the top cap. Circumference strain, ε_θ, and radial strain, ε_r, are calculated from the changes in the inner and outer radii of the specimen which are obtained from volume changes of the specimen itself and the hollow of the specimen. The volume changes are measured as the changes of weight of water in the specimen and the hollow by using electrical balances kept in chambers to supply the back pressure and the inner cell pressure respectively. Corrections to the volume changes are made for the membrane penetration and for the change in the thickness of the inner membrane. With those measurement systems and corrections, small strains of the order of 10^{-3}% can be measured precisely for all the strain components (Nakamura et al. 1999).

Toyoura sand specimens with the relative density of about 80% were made by air pluviation. Index properties of Toyoura sand are D_{50}=0.15 mm, G_s=2.645, e_{min}=0.609 and e_{max}=0.973. The sample was saturated by vacuuming and applying the back pressure of 196 kPa. Then, it was consolidated isotropically at p' = 98.1 kPa for about 6 hours. After the isotropic consolidation, the specimen was sheared keeping the mean effective stress, p', and the intermediate principal stress parameter, b, constant so as

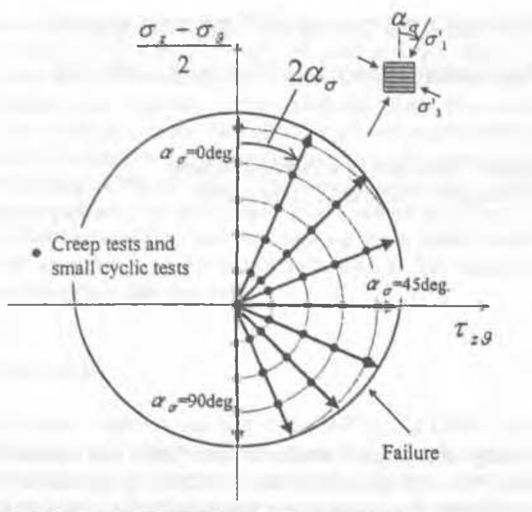

Figure 2. Schematic illustration of shear process.

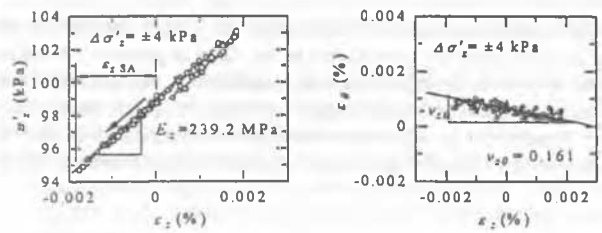

Figure 3. Example of small cyclic loading test result.

to be 98.1 kPa, and 0.5 respectively. The shear process is schematically illustrated in Figure 2.The angle, α_σ, between the σ_1 axis and the vertical was also kept constant to be 0, 11.25, 22.5, 33.75, 45, 56.25, 67.5, 78.75 or 90° during shearing. At certain level of the maximum shear stress, τ_{max}, the stress condition was maintained constant and the creep strain was observed. The increment rate of the maximum shear stress, $\Delta\tau_{max}/\Delta t$, in the monotonic shear stage was about 0.3 kPa/min. When the creep deformation had almost terminated with the maximum shear strain rate, $\Delta\gamma_{max}/\Delta t$, of less than about 10^{-4} %/min., cyclic stresses $\Delta\sigma'_z$, $\Delta\sigma'_\theta$ and $\Delta\tau_{z\theta}$ of amplitude ±2 and ±4 kPa were applied to the specimen to obtain the small-strain stiffness, E_z, E_θ and $G_{z\theta}$. The example is shown in Figure 3. The strain rate in this small amplitude cyclic shear was about 10^{-3} %/min. Measurements of Poisson's ratio were made at this stage as well. Small-strain deformation characteristics were also measured in the isotropic stress state of p' = 29.4~196 kPa.

3 RESULTS AND DISCUSSIONS

3.1 *Creep strain rate*

At certain constant stress levels in monotonic shearing, strains were observed to increase with time. The amount of creep strain was larger for the higher shear stress levels, for example, as large as γ_{max} of about 0.2% was observed at the maximum shear stress ratio, τ_{max}/τ_{maxf}, of 0.720 after approximately 100 minutes in case of α_σ=56.25° shear. τ_{maxf} is the maximum shear stress at failure in that directional shear. From the plotting of the maximum shear strain rate, $\Delta\gamma_{max}/\Delta t$, against time, t, in log-log scale as shown in Figure 4, the following linear relationships were obtained for the respective shear levels:

$$\ln\Delta\gamma_{max}/\Delta t = m + n\ln t/t_1 \qquad (1)$$

where m and n are parameters and are not affected by α_σ. t_1 in Equation 1 is a reference time and 1 min. was used in this study.

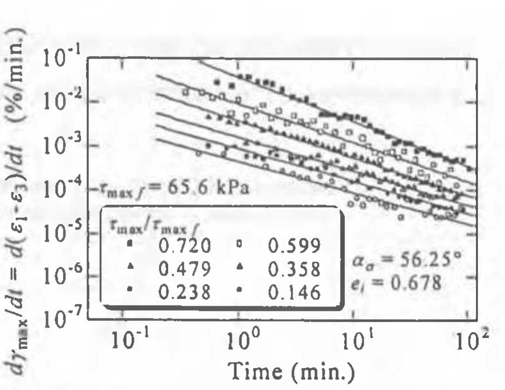

Figure 4. Variation of strain rate with time.

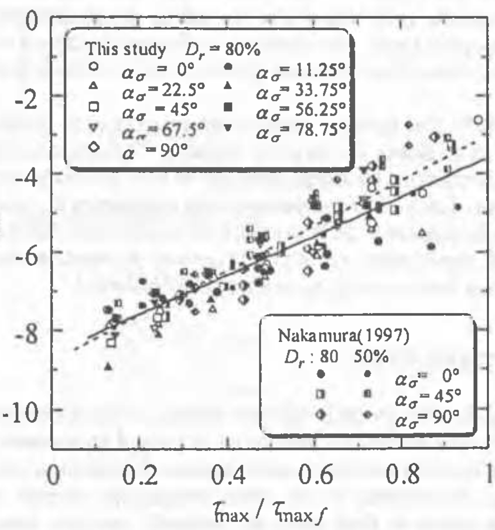

Figure 5. Creep parameter m vs. shear stress level τ_{max}/τ_{maxf}.

Parameter m increases almost linearly with the shear stress level, τ_{max}/τ_{maxf}, but does not depend much on the major principal stress direction, α_σ. However, n depends little on τ_{max}/τ_{maxf} nor α_σ. Therefore, m and n are written as follows:

$$m = a_1 + b_1\frac{\tau_{max}}{\tau_{max f}} = -8.59 + 5.01\frac{\tau_{max}}{\tau_{max f}} \qquad (2)$$

$$n = -0.75 \qquad (3)$$

Substitution of m and n as above into Equation 1 gives:

$$\frac{d\gamma_{max}}{dt} = \left(\frac{t}{t_1}\right)^n \exp\left(a + b\frac{\tau_{max}}{\tau_{max f}}\right) \qquad (4)$$

Rate of the maximum creep shear strain given by this equation is a function of t and τ_{max}/τ_{maxf}, but not affected by α_σ as mentioned above. Equation 4 has the same form as the equation to describe the creep behavior of soil derived from the rate-process theory (Feda 1992) or the rheological model (Murayama 1983).

3.2 *Direction of the creep strain*

Directions of the major principal creep strain, α_ε^c, were monitored and plotted against the time as shown in Figure 6. This was determined for the total creep strain components from the start of

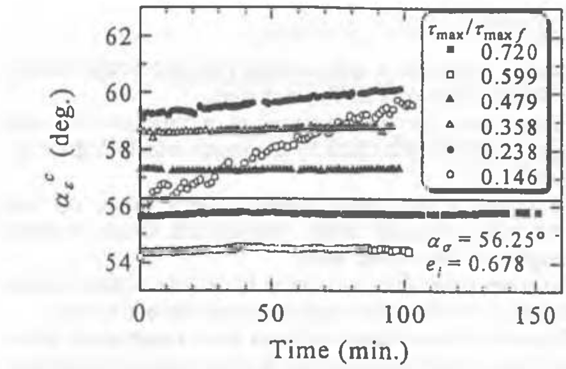

Figure 6. Change in the direction of the major principal creep strain with time.

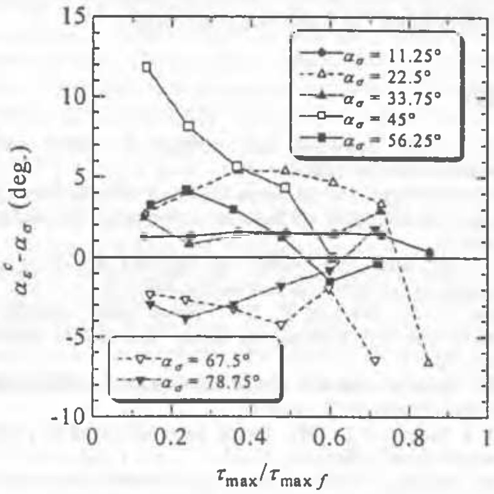

Figure 7. α_ε^c -α_σ versus τ_{max}/τ_{maxf}.

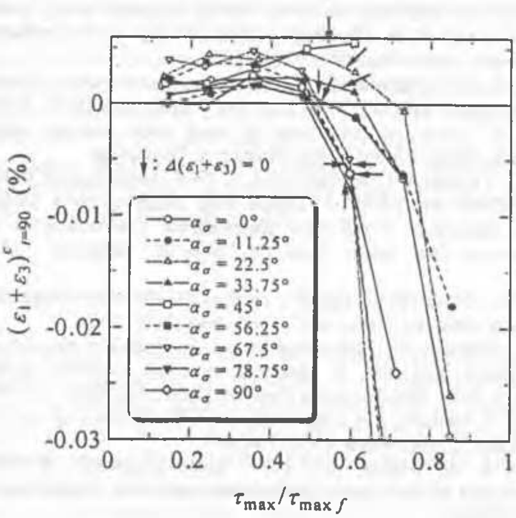

Figure 8. Creep volumetric strain versus shear stress level.

the creep process, and not for the incremental components. It is seen that the directions, α_ε^c, are around the major principal stress direction and almost constant for the respective shear stress levels, τ_{max}/τ_{maxf}, except at the very low shear stress level. They depended on the direction of the major principal stress in the monotonic shear, α_σ, as well as the shear stress level, τ_{max}/τ_{maxf}.

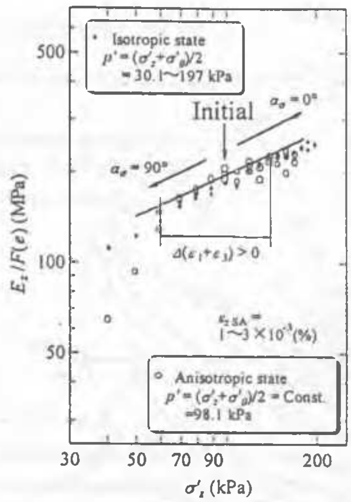

Figure 9. Stress dependency of E_z on normal stress.

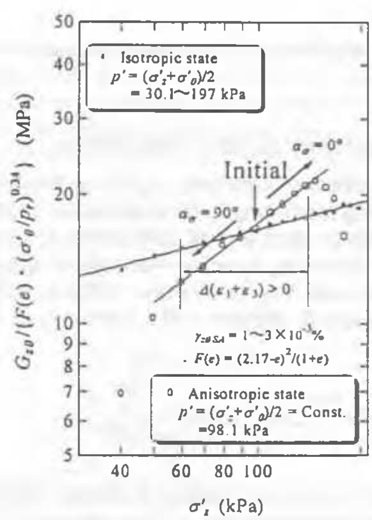

Figure 10. Stress dependency of $G_{z\theta}$ on normal stresses.

Differences between the major principal direction of stress and that of creep strain, α_ε^c -α_σ, are plotted in Figure 7 against the shear stress level for the respective shear directions. Although there are some scatters, the creep strain directions seem to deviate toward the direction of 60° from the major principal stress direction. α_ε^c is within about plus or minus 5 degrees from α_σ and seems to approach α_σ with shearing maybe owing to the effects of induced anisotropy.

3.3 *Creep volumetric strain*

Although shearing was done with constant p', some creep volumetric strain was registered. Similar to the ordinary volume change tendency, creep volumetric strain in z-θ plane, $(\varepsilon_1+\varepsilon_3)^c$, was contractive for lower shear stress level, and became dilative with the increase in the shear stress level as shown in Figure 8, where $(\varepsilon_1+\varepsilon_3)^c_{t=90}$ is creep volumetric strain at t=90min when the creep deformation almost terminates. Such a change in the creep volumetric strain characteristic appeared in the earlier stage of shearing for the horizontal compression with α_σ=56.25~90° than for the vertical compression with α_σ=0~45°. At the point of zero dilatancy, $\Delta(\varepsilon_1+\varepsilon_3)$=0, in overall shearing, the creep volumetric strain was still contractive for the vertical compression, whereas it was already dilative for the horizontal compression.

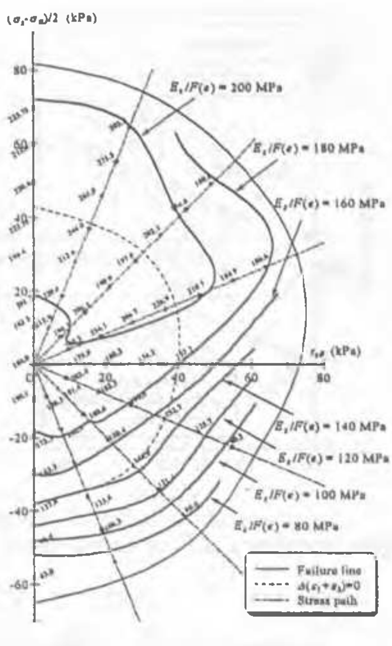

Figure 11. Contour lines of E_z in constant p' plane.

3.4 *Stress dependency of small strain stiffness*

Small-strain stiffness components, E_z, E_θ and $G_{z\theta}$, were measured by applying small amplitude cyclic loads at certain stress levels in monotonic shear as well as in isotropic stress states. In this study, the following equation was used to approximate the relationship between the small-strain stiffness and the stress condition (Viggiani & Atkinson 1995, Bellotti et al. 1996). If for $G_{z\theta}$:

$$\frac{G_{z\theta}}{p_r} = C_{z\theta}F(e)\left(\frac{\sigma'_z}{p_r}\right)^{n_z}\left(\frac{\sigma'_\theta}{p_r}\right)^{n_\theta} f\left(\frac{\tau_{z\theta}}{p_r}\right) \quad (5)$$

where $F(e)=(2.17-e)^2/(1+e)$ (Hardin & Richart 1963) and 1 kPa is used for the reference stress, p_r. The value of E_z for the isotropic stress condition ($\sigma'_\theta = 98.1$ kPa) was practically same as E_z in anisotropic stress conditions ($\sigma'_\theta >$ or $<$ 98.1 kPa) in the region of volume contraction, $\Delta(\varepsilon_1+\varepsilon_3)>0$. However, in the dilatant region, $\Delta(\varepsilon_1+\varepsilon_3)<0$, E_z decreased rapidly with shear as shown in Figure 9. E_z depends little on σ'_θ, but varies with σ'_z in proportion to $(\sigma'_z)^{0.5}$, i.e. n_z=0.5 and n_θ=0. On the other hand, E_θ did not depend on σ'_z, but varied with σ'_θ in proportion to $(\sigma'_\theta)^{0.5}$, i.e. n_z=0 and n_θ=0.5. $G_{z\theta}$ increased with both σ'_z and σ'_θ, i.e. $(\sigma'_z)^{nz}(\sigma'_\theta)^{n\theta}$, as seen in Figure 10, but did not depend much on $\tau_{z\theta}$. n_z decreased from 0.618 to 0.509 whereas n_θ increased from 0.341 to 0.454, when σ_1 direction, α_σ, changed from 0° to 33.75°. $G_{z\theta}$ is affected more by the normal stress whose direction is closer to that of σ_1 than the other normal stress component.

Contours of E_z, E_θ and $G_{z\theta}$ can be drawn on the $\tau_{z\theta}$-$(\sigma_z$-$\sigma_\theta)/2$ shear plane (p'-constant plane) to see overall shear stress dependency of small-strain stiffness. Figure 11 is the contour lines of E_z for example. E_z decreases more rapidly in the extension side, i.e. α_σ=45~90°, than the compression side. E_θ shows opposite trend. The modulus shows rapid decrease near failure indicating deterioration of soil structure.

Poisson's ratio was also measured. Although there were some scatters, it was about 0.1~0.15 and did not show clear dependency on α_σ or τ_{max}/τ_{maxf}.

4 CONCLUSIONS

The following conclusions were derived from a series of hollow cylinder torsion shear tests on Toyoura sand.

1. Creep strain rate is expressed as a function of t and τ_{max}/τ_{maxf}, but not affected much by the major principal stress direction, α_σ.

2. Directions of the major principal creep strain, α_ε^c, are around the major principal stress direction and almost constant for the respective shear stress level.

3. The creep strain directions seem to deviate slightly toward the direction of 60° from the major principal stress direction.

4. The value of small-strain stiffness for the anisotropic stress condition is practically same as that for the isotropic stress condition in the region of volume contraction. It increases with the increase in the normal stress. However, in the dilatant region, it decreases rapidly with shear.

5. Contours of small-strain stiffness, E_z, E_θ and $G_{z\theta}$, are drawn on the $\tau_{z\theta}$-$(\sigma_z$-$\sigma_\theta)/2$ shear plane (p'-constant plane) to see overall shear stress dependency of small-strain stiffness.

REFERENCES

Atkinson, J.H. 2000. Non-linear soil stiffness in routine design. *Géotechnique* 50(5): 487-508.

Bellotti, R., Jamiolkowski, M., Lo Presti, D.C.F. & O'Neill, D.A. 1996. Anisotropy of small strain stiffness in Ticino sand. *Geotechnique* 46(1): 115-131.

Burland, J.B. 1989. Small is beautiful - the stiffness of soils at small strains. *Canadian Geotechnical Journal* 26: 499-516.

Di Benedetto, H. & Tatsuoka, F. 1997. Small strain behavior of geomaterials: modelling of strain rate effects. *Soils and Foundations* 37(2): 127-138.

Feda, J. 1992. *Creep of soils and related phenomena*. Developments in geotechnical engineering 68, Elsevier.

Hardin, B.O. & Richart, F.E. 1963. Elastic wave velocities in granular soils. *Journal of ASCE* 89(SM1): 33-65.

Hoque, E. & Tatsuoka, F. 1998. Anisotropy in elastic deformation of granular materials. *Soils and Foundations* 38(1): 163-179.

Jovicic, V. & Coop, M.R. 1998. The measurement of stiffness anisotropy in clays with bender element tests in triaxial apparatus. *Geotechnical Testing Journal* 21(1): 3-10.

Kuwano, R., Connolly, T.M., Jardine, R.J. & Kuwano, J. 1997. Shear wave velocity measurements in the triaxial apparatus using lateral bender elements. *Proc. 32nd Japan National Conf. on Geotechnical Engineering, Kumamoto*, JGS 1: 809-810.

Murayama, S. 1983. Formulation of stress-strain-time behavior of soils under deviatoric stress cindition. *Soils and Foundations* 26(4): 79-97.

Nakamura, Y. Study on anisotropy of sand under various stress conditions. *Master Thesis*, Tokyo Institute of Technology.

Nakamura, Y., Kuwano, J., & Hashimoto, S. 1999. Anisotropy of small-strain stiffness and creep of Toyoura sand measured by a hollow cylinder apparatus. *Pre-Failure Deformation Characteristics of Geomaterials*; *Proc. Intern. Symp. (IS-Torino'99)*. Balkema, 1: 141-148.

Oda, M. 1972. Initial fabrics and their relation to mechanical properties of granular materials. *Soils and Foiundations* 12(1): 18-36.

Shibuya, S., Tatsuoka, F., Teachavorasinskun, S., Park, C.S. & Abe, F. 1991. Elastic properties of granular materials measured in the laboratory. *Proc. 10th European Conf. on SMFE, Florence*: 163-166.

Viggiani, G. & Atkinson, J.H. 1995. Stiffness of fine-grained soil at very small strains. *Geotechnique* 45(2): 249-265.

Zdravkovic, L. & Jardine, R.J. 1997. Some anisotropic stiffness characteristics of a silt under general stress conditions. *Geotechnique* 47(3): 407-437.